S-functionalized MXenes as electrode materials for Li-ion batteries

Zhu, J, Chroneos, A, Eppinger, J & Schwingenschlögl, U

Original citation & hyperlink:
Zhu, J, Chroneos, A, Eppinger, J & Schwingenschlögl, U 2016, 'S-functionalized MXenes as electrode materials for Li-ion batteries' *Applied Materials Today*, vol 5, pp. 19-24
https://dx.doi.org/10.1016/j.apmt.2016.07.005

DOI 10.1016/j.apmt.2016.07.005
ISSN 0264-9993

Publisher: Elsevier

S-functionalized MXenes as Electrode Materials for Li-Ion Batteries

Jiajie Zhu[1], Alexander Chroneos[2,3,a], Jörg Eppinger[1], and Udo Schwingenschlögl[*,1,b]

[1]PSE Division, KAUST, Thuwal 23955-6900, Kingdom of Saudi Arabia

[2]Department of Materials, Imperial College, London SW7 2AZ, United Kingdom

[3]Faculty of Engineering and Computing, Coventry University, Priory Street,

Coventry CV1 5FB, United Kingdom

[a]Email: ab8104@coventry.ac.uk

[b]Email: udo.schwingenschlogl@kaust.edu.sa

September 27, 2016

Abstract

MXenes are promising electrode materials for Li-ion batteries because of their high Li capacities and cycling rates. We use density functional theory to investigate the structural and energy storage properties of Li decorated Zr_2C and Zr_2CX_2 (X = F, O and S). We find for Zr_2C and Zr_2CS_2 high Li specific capacities and low diffusion barriers. To overcome the critical drawbacks of the OH, F, and O groups introduced during the synthesis we propose substitution by S groups and demonstrate that an exchange reaction is indeed possible. Zr_2CS_2 shows a similar Li specific capacity as Zr_2CO_2 but a substantially reduced diffusion barrier.

Keywords: Zr_2C, MXene, Functionalization, Li-ion battery, Capacity, Diffusion

1 Introduction

Numerous two-dimensional materials, including boron nitride,[1] transition metal chalcogenides,[2] and silicene,[3] are products of the graphene era.[4–6] MXenes[7–11] form a rather new class of two-dimensional carbides and/or carbonitrides[12] with numerous potential applications in sensors, electronic devices, optoelectronic devices, supercapacitors, or as catalyst materials.[13–18] MXenes are commonly synthesized by selective etching of the A metal from the three-dimensional $M_{n+1}AX_n$ phases (where n = 1,2,3,4, M is an early transition metal, A is a group 13-16 element, and X is C and/or N).[19,20] The $M_{n+1}AX_n$ phases have hexagonal structures (space group $P63/mmc$), which are composed of n "ceramic" MX layer(s) alternating with the "metallic" A layer. The combination of ceramic (high decomposition or melting temperature, high elastic stiffness, and good machinability) and metallic (high thermal shock resistance and good thermal and electrical conductivities) characteristics leads to widely applicable materials.

The main drive for the investigation of MXenes as electrode materials for Li-ion batteries is the high Li storage capacity, which is comparable to the commercial graphite electrodes.[21] Small Li diffusion barriers additionally result in high cycling rates.[21,22] Most metallic MXenes provide a high electrical conductivity.[23] Ti_2C has been predicted to be stable during the Li adsorption process[24] and dimethylsulfoxide intercalation has been demonstrated to improve the Li capacity of Ti_3C_2.[25] Concerning materials simulations, Xie and Kent[26] have shown that the Perdew-Burke-Ernzerhof (PBE) and Heyd-Scuseria-Ernzerhof (HSE06) functionals result in similar structural and electronic properties for $Ti_{n+1}C_n$ (n = 1 to 9), even though the HSE06 functional often is deemed to be more accurate.

Although the MXene family grows continuously and consists of various types of compounds (M = Sc, Ti, V, Cr, Zr, Nb, Hf, and Ta),[27,28] only the titanium carbides have been investigated systematically.[21,24–26,29] Reports on the performance of other MXenes are scarce. In the case of V_2C a Li capacity of 941 mAh/g has been predicted when considering multilayer Li adsorption, which is considerably higher than the experimental value of 260 mAh/g.[30] The successful preparation of $Zr_{n+1}AX_n$ phases[31,32] paves the way to Zr-based MXenes, as the synthesis of MXenes from the respective bulk materials is well established. Indeed, Zr-based MXenes are likely to be realized more easily than their Ti and Nb counterparts because of larger differences in the bonding strength within the *ab*-plane and along the *c*-axis.[33] Inevitably, OH, F, and O groups cap the MXene during

preparation due to the presence of HF and H_2O.[34] These hard nucleophiles may bind to Li to form byproducts, which obstruct Li diffusion.[35] In the present study we investigate the applicability of Zr_2C, a material that so far has escaped attention, for Li-ion batteries, focusing on new capping elements, including S, Se, and Te.

2 Computational method

The calculations are performed in the framework of density functional theory using the projector augmented wave method as implemented in the Vienna Ab-initio Simulation Package.[36] The generalized gradient approximation (PBE flavor) is selected for the exchange-correlation potential.[37] Brillouin zone integrations are performed on $6 \times 6 \times 1$ and $12 \times 12 \times 1$ k-meshes, respectively, for the geometry optimization and electronic structure calculations. A cut-off energy of 500 eV for the plane wave basis is found to yield converged results. The energy criterion for the iterative solution of the Kohn-Sham equations is set to 10^{-6} eV. All structures are relaxed until the residual forces on the atoms have declined to less than 0.01 eV/Å. A $2 \times 2 \times 1$ supercell of monolayer Zr_2C is used to model Li decoration, where a vacuum layer of 15 Å thickness is found to be sufficient to avoid unphysical interaction between images due to the periodic boundary conditions. We have tested for the Li diffusion barriers that the results for a $3 \times 3 \times 1$ supercell deviate by less than 5%. The nudged elastic band method[38] with 7 to 9 images between the initial and final configurations is applied to calculated the energy barriers of Li diffusion and thus to determine the minimum energy paths.

Reaction enthalpies $\Delta_r H$ are derived form the computed bulk/molecular total energies of the reactants and products: -41.203 eV for Zr_2CF_2, -47.358 eV for Zr_2CO_2, -40.087 eV for Zr_2CS_2, -32.656 eV for S_8, -3.557 eV for F_2, -9.858 eV for O_2, -22.953 eV for CO_2, -16.220 eV for CS_2, -19.828 eV for COS, -11.202 eV for H_2S, and -14.219 eV for H_2O. The cohesive energy of Zr_2CS_2 is calculated to be 4.95 eV/atom, reflecting chemical stability. Gibbs energies $\Delta_r G$ are calculated using the gas phase entropies at the respective temperatures, which are available from the NIST database, except for the MXenes.[39] We assume that i) an entropic contribution of the MXenes to the overall thermochemistry of the conversions can be neglected due to very similar compositions and structures, ii) all reactants are in the gas phase with the exception of the solid MXenes, which is reasonable as similar conversions typically require elevated temperatures and gaseous reactants can well access the MXene surface, and iii) $\Delta_r H$ is constant within a synthetically reasonable temperature range.

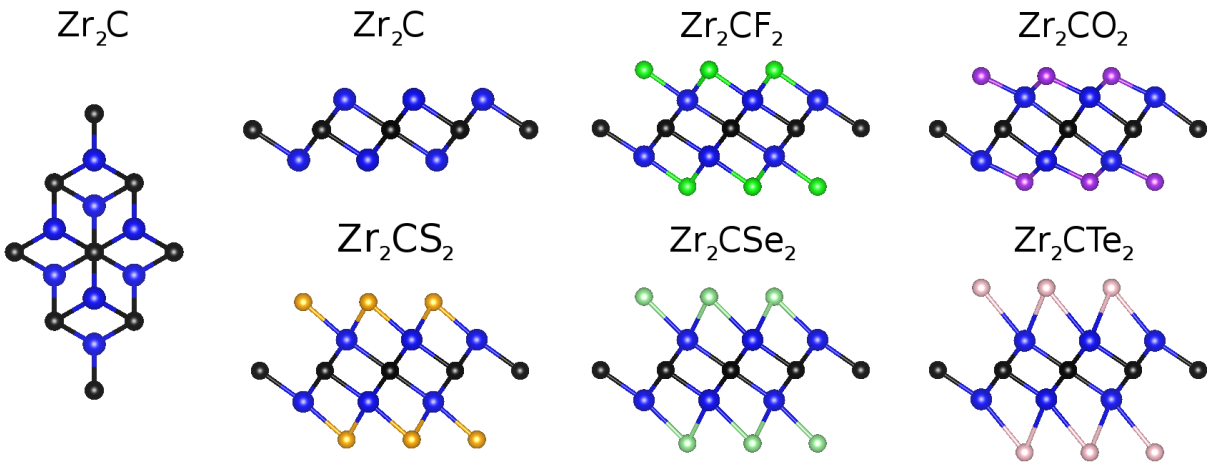

Figure 1: Structures of Zr_2C and Zr_2CX_2 (X = F, O, S, Se, and Te) (left: top view, others: side view). The Zr, C, F, O, S, Se, and Te atoms are shown in blue, black, green, purple, brown, cyan, and pink color.

Applying available gas phase enthalpy corrections,[39] $\Delta_r H$ changes by less than 1.4 kcal/mol between 300 and 1000 K.

3 Results and discussion

Figure 1 shows the structures of Zr_2C and Zr_2CX_2 (X = F, O, S, Se, and Te). Non-magnetic, ferromagnetic, and antiferromagnetic calculations are performed in the case of the bare MXene. Antiferromagnetism with parallel spins within each Zr layer but opposite spins in the top and bottom Zr layers is found to constitute the ground state (10 meV per atom lower energy than ferromagnetism), which contradicts previous calculations[28] that have used a weaker energy criterion for the self-consistency (10^{-4} eV). The in-plane lattice constant of Zr_2C is calculated to be 3.317 Å, which is in agreement with a previous theoretical result (3.269 Å).[40] Added capping elements can be located on top of the C, Zr(1) (top Zr layer), and Zr(2) (bottom Zr layer) atoms, on both sides of the MXene. All groups favor to be located on top of the C atoms (coordinated equidistantly to three neighbouring Zr atoms), which results in a non-magnetic state. The Zr(1)-X bond lengths are calculated to be 2.12, 2.53, 2.69, and 3.01 Å for O, S, Se, and Te functionalization, respectively, reflecting the different ionic radii. The Zr-F bond (2.33 Å) is longer than the Zr-O bond due to the different oxidation states of the anionic capping elements. The higher negative charge of the O group results in a stronger Coulombic interaction to the positively charged Zr atoms.

Li can be located on top of the C, Zr(1), and Zr(2)/X atoms. Energetical favorable is Zr(2) for

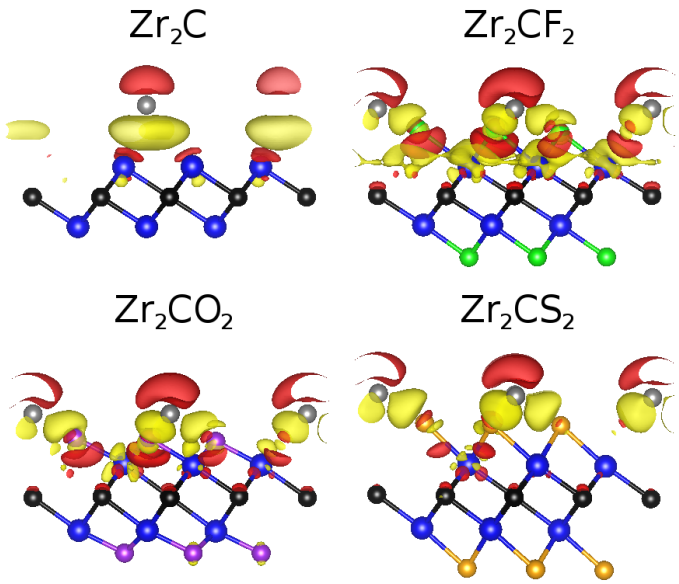

Figure 2: Charge redistribution due to the interaction with Li. Yellow/red color represents charge accumulation/depletion, where the isosurfaces refer to an isovalue of 2×10^{-3} electrons/bohr^3. The Zr, C, Li, F, O, and S atoms are shown in blue, black, grey, green, purple, and brown color.

the bare MXene, C for F/O/S passivation, and Zr(1) for Se/Te passivation. The Li-X bond lengths are calculated to be 1.86, 2.04, 2.29, 2.41, and 2.62 Å for F, O, S, Se, and Te, respectively, due to increasing atomic radii. The stability of a phase is given by its formation energy with respect to a reference material,

$$\Delta H = E - E_{\mathrm{MXene}} - E_{\mathrm{reference}}, \tag{1}$$

where E is the total energy of the full system, E_{MXene} the total energy of the MXene without Li, and $E_{\mathrm{reference}}$ the total energy of the reference material (bulk Li and Li_2X). The capping atoms may form byproducts with Li. For the F group and one Li atom with respect to LiF and the O, S, Se, and Te groups and two Li atoms with respect to Li_2X (X = O, S, Se, and Te) we obtain formation energies of -0.25, -2.62, -1.06, 0.55, and 2.88 eV, respectively. Negative values indicate an exothermic process. The instability of the Se and Te terminations when Li atoms are added is a consequence of the larger Zr-Se and Zr-Te bond lengths. Since capping with Se and Te atoms is unstable in Li environment, these cases will not be considered in the following. For decoration with a single Li atom with respect to bulk Li we obtain values of -0.34, -1.05, -1.70 and -2.07 eV for Zr_2C and Zr_2CX_2 (X = F, O and S), respectively. The positive value of 0.88 eV in the case of $Zr_2C(OH)_2$ points to the formation of Li clusters.[35]

Further insight into the stability can be obtained from the charge density differences shown in

Table 1: Partial atomic charges (in electrons) calculated by the Bader approach for Zr_2C and Zr_2CX_2 (X = F, O, and S).

	bare	F	O	S
Li	+0.81	+0.88	+0.87	+0.86
X		−0.85	−1.35	−1.08
Zr(1)	+0.82	+1.74	+2.15	+1.84
C	−2.19	−2.14	−1.98	−1.94

Figure 2, defined as

$$\Delta\rho = \rho - \rho_{\mathrm{MXene}} - \rho_{\mathrm{Li}}, \tag{2}$$

where ρ, ρ_{MXene}, and ρ_{Li} are the charge densities of the full system, the MXene without Li, and an isolated Li atom, respectively. In the case of the bare MXene the charge redistribution towards Li is significantly different from the cases of the passivated MXenes, reflecting differences in the interaction. For the passivated MXenes, the charge redistribution becomes smaller from F to S because of the decreasing electronegativity. Mostly the Zr(1) and X (X = F, O, and S) atoms are affected. Table 1 lists partial atomic charges calculated by the Bader approach. A higher charge redistribution indicates a stronger polarization of the electronic shells of the X atoms and this in turn an enhanced covalency for the X-Li interaction, which explains the less negative formation energy for Li decoration described above. The densities of states shown in Figure 3 demonstrate increasing hybridization between the X p and Li s states (enhanced covalent interaction) from X = F to S.

The charging rate depends on the diffusion properties of Li. Three diffusion paths are considered, where the ground state position of Li and its nearest neighbor positions are the initial and final states. Path I/II passes the top of the C/Zr(1) and Zr(1)/X atoms, respectively, for the bare and F/O/S passivated MXenes, whereas path III directly connects the initial and final states. Path I, see Figure 4, exhibits a lower diffusion barrier than path II for all cases due to the strong interaction at the transition states. Path III always converges to path I. The diffusion barrier for Li along path I is compared in Figure 5. Zr_2C shows the lowest value of 34 meV due to flat a surface charge distribution with the transition state located on top of the Zr(2)-C bond. There is a local minimum (17 meV) on top of the C atom. In the other cases the diffusion barriers are much higher, where the transition state is located on top of the Zr(1) atom for Zr_2CO_2 and on top of the Zr(1)-C bond for Zr_2CF_2 and Zr_2CS_2. Presence of many OH groups can be expected because of the synthesis in water.[41] Although this group can be converted into an O group by high temperature annealing to improve the Li stability,[35] the semiconducting character[23] and high diffusion barrier still limit the

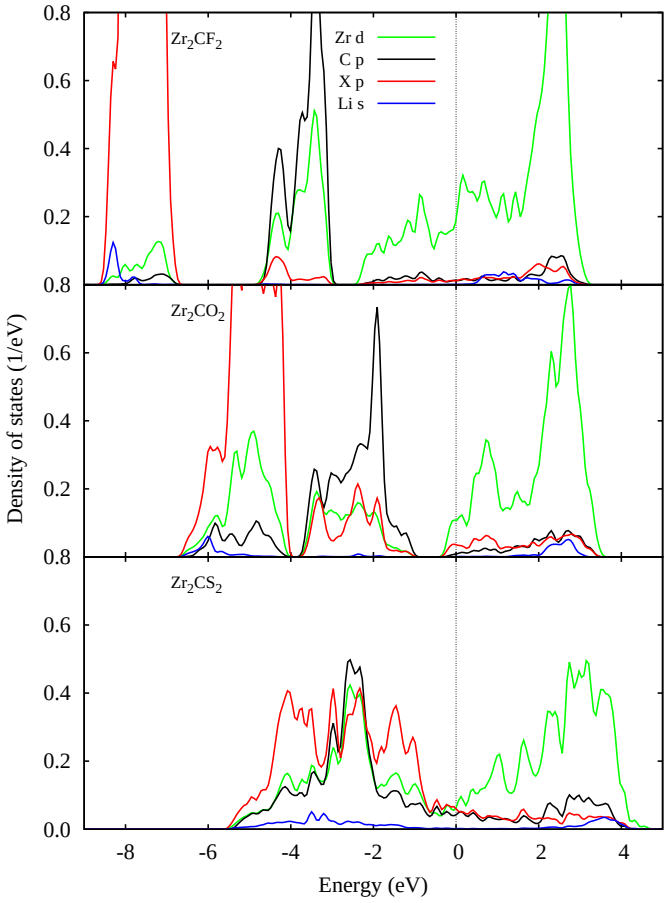

Figure 3: Densities of states for Zr_2CX_2 (X = F, O, and S) after Li decoration. The Fermi level is set to zero.

applicability of the material. In contrast, Zr_2CS_2 is found to be metallic, which is crucial for battery applications.

However, our calculations indicate that exchanging the OH, F, and O groups on the Zr_2C surface sheet for S should overcome these drawbacks. We expect that such an exchange should indeed be experimentally feasible. Qualitatively, the conductive Zr_2C has a high electron density and correspondingly the Zr atoms should be considered rather soft Lewis metal centers unlike the Zr(IV) ions in typical Zr salts, resulting in a preference for the soft S over the hard F and O anions. To evaluate which reagent might allow the synthesis of Zr_2CS_2, we estimate the thermochemistry for conversions of the respective MXenes from a combination of computational and experimental data.[39]

Concerning the interconversions of the MXenes with elemental S, we find strongly endothermic reactions

$$Zr_2CX_2 + 1/4 \cdot S_8(g) \rightarrow Zr_2CS_2 + X_2(g)$$

132/128 kcal/mol for X = F/O. A temperature above 600 K would be required to achieve a reasonable

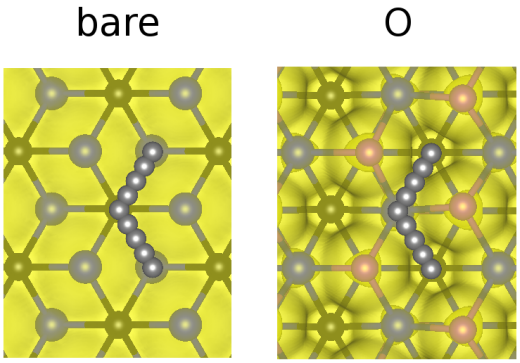

Figure 4: Diffusion paths for Li atoms. The Zr, C, Li, and F/O/S atoms are shown in blue, black, grey, and purple color. The surface charge distribution is shown in yellow for the O case. For the F and S cases the distribution is virtually the same.

vapor pressure of S_8 (and smaller S_n molecules) in the gas phase.[42] For X = F/O we obtain $\Delta_r G$ values of 125/121 kcal/mol at 298 K, 119/115 kcal/mol at 600 K, and 115/112 kcal/mol at 800 K. Correspondingly, a reagent with a strongly exergonic S/O-exchange is necessary to drive the reaction. H_2S as S transfer reagent cannot provide the free energy required

$$2H_2S + O_2 \rightarrow 2H_2O(g) + 1/4 \cdot S_8(g),$$

$\Delta_r H^0 = -99.9$ kcal/mol, $\Delta_r G^0 = -91.4$ kcal/mol) so that a treatment of the MXenes with H_2S is not sufficient. A more exothermic S/O-exchange reagent should react with water under release of H_2S. CS_2 is known to hydrolyze[43,44] under formation of CO_2 and H_2S. Its formal conversion to COS

$$2CS_2(g) + O_2 \rightarrow 2COS + 1/4 \cdot S_8(g),$$

$\Delta_r H^0 = -127.2$ kcal/mol, $\Delta_r G^0 = -119.8$ kcal/mol) can provide the necessary free energy. The interconversion of Zr_2CO_2 with CS_2 to Zr_2CS_2 under the release of COS should therefore be nearly thermoneutral and feasible, for example by applying an excess of S. The calculated $\Delta_r G$ for this reaction is 1.7 kcal/mol at 298 K, 2.6 kcal/mol at 600 K, and 3.2 kcal/mol at 800 K. The exchange of both S atoms in CS_2 for O is slightly less exothermic

$$CS_2(g) + O_2 \rightarrow CO_2 + 1/4 \cdot S_8(g),$$

$\Delta_r H^0 = -116.0$ kcal/mol, $\Delta_r G^0 = -107.4$ kcal/mol) so that the Zr_2CO_2/Zr_2CS_2 interconversion

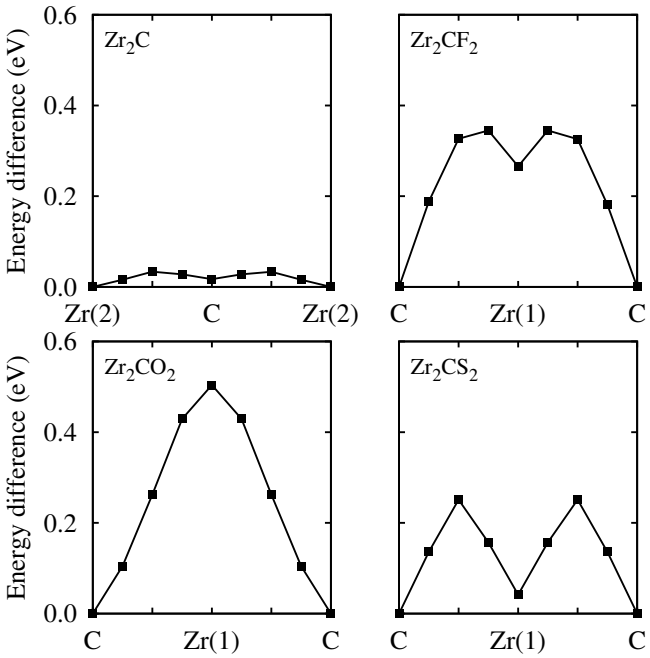

Figure 5: Diffusion barriers for Li atoms on Zr_2C and Zr_2CX_2 (X = F, O, and S).

under the release of CO_2 is moderately endergonic (14.1 kcal/mol at 298 K, 16.7 kcal/mol at 600 K, and 18.5 kcal/mol at 800 K). Literature provides evidence that the above reactions are kinetically feasible. CS_2 has a rich chemistry with transition metals and readily inserts into MO bonds.[45] Correspondingly, CS_2 has been used as a less toxic replacement of H_2S in the preparation of metal-sulfides form oxides, for example in the synthesis of ZrS_2,[46] the full or partial S/O-exchange in spinel $Li_4Ti_5O_{12}$, and the preparation of other transition metal sulfides.[47–49]

A high Li specific capacity (ability to absorb Li atoms) is crucial for usage of MXenes as anode material. We consider adsorption up to a monolayer of Li on both sides of the MXene as our aim is to demonstrate the effects of the functional group. The real capacity will be higher, because the Li atoms can arrange in multilayers.[30] The open circuit voltage as a function of the Li coverage is addressed in Figure 6. For Zr_2CLi_x the voltage is approximately 0.4 V, $Zr_2CO_2Li_x$ delivers a maximal voltage of 2.5 V when 3 Li atoms are located on each side of the MXene ($x = 1.5$), and the voltage decreases continuously for $Zr_2CS_2Li_x$. Zr_2CS_2 can absorb up to 10 Li atoms per $2 \times 2 \times 1$ supercell without forming clusters, see Figure 7, where 8 are located on top or bottom of C atoms and 2 on top of Zr(1) atom, corresponding to 2.5 Li atoms per unit cell. Zr_2C and Zr_2CO_2 can accommodate 9 Li atoms (2.25 Li atoms per unit cell), whereas Zr_2CF_2 can accommodate only 2 Li atoms without

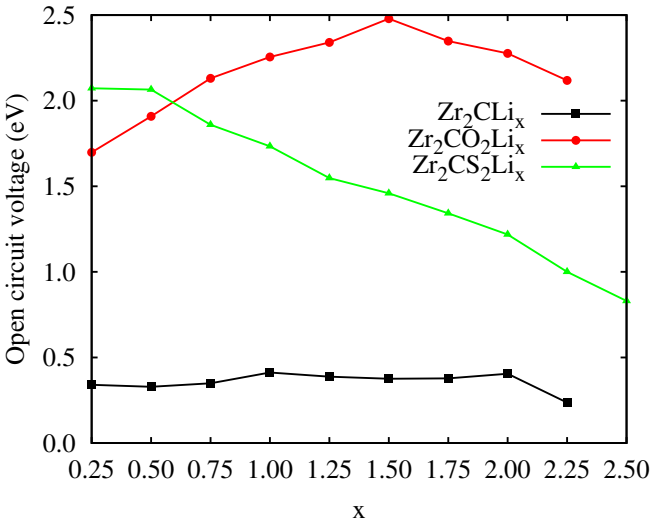

Figure 6: Open circuit voltage for Zr_2C and Zr_2CX_2 (X = O and S) as a function of the Li coverage.

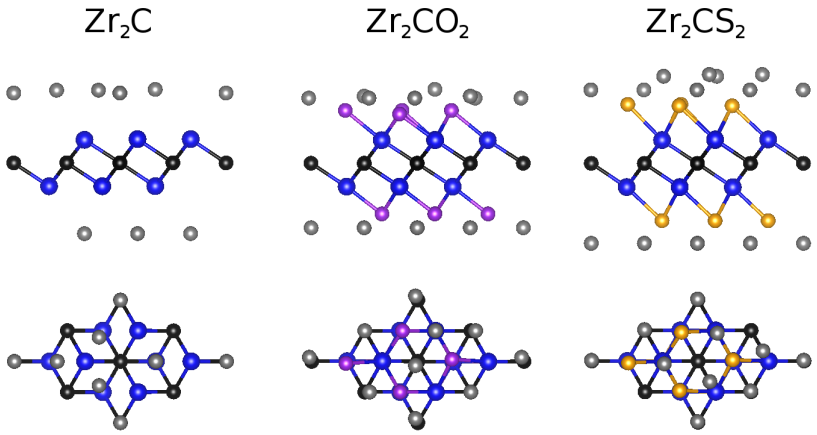

Figure 7: Side and top views of fully lithiated Zr_2C, Zr_2CO_2, and Zr_2CS_2. The Zr, C, O, S, and Li atoms are shown in blue, black, purple, brown, and grey color.

forming LiF, as reported previously for Ti_3C_2 and V_2C.[22,30] The Li specific capacity is given by

$$C = \frac{x \cdot F}{M}, \tag{3}$$

where M is the atomic mass of Zr_2CX_2 and F is the Faraday constant. We obtain 310 mAh/g for Zr_2C, 266 mAh/g for Zr_2CO_2 and 259 mAh/g for Zr_2CS_2. These values are comparable to the high Li specific capacity of Ti_3C_2 (320 mAh/g).[22] A much lower value of 58 mAh/g is obtained for Zr_2CF_2. Importantly, the S group provides a similar performance as the O group.

4 Conclusions

Our comparative study of Li decoration of Zr_2C and Zr_2CX_2 (X = OH, F, O, S, Se, and Te), for evaluating possibilities and limitations of application in Li-ion batteries shows that the charge redistribution at the interface between Li and the functional group of the MXene decreases from F to S, following the electronegativity trend. Li specific capacities of 310 and 259 mAh/g are obtained for Zr_2C and Zr_2CS_2, respectively, which are very promising values. Zr_2CS_2 shows a substantially reduced diffusion barrier but similar Li specific capacity as Zr_2CO_2. Nowadays OH, F, and O groups attached to the surface are inevitable during the preparation of MXenes. Their replacement with S groups is predicted to result in high electric conductivities and cycling rates (minor structural distortions, low diffusion barriers) for Li-ion batteries using Zr-based MXenes. In addition, byproducts affecting the lifetime are avoided. Importantly, the replacement is compatible with present synthesis techniques, since it can be applied to the as-prepared MXenes. While OH groups can be converted into O groups by high temperature annealing, O and F groups can be replaced by S groups via moderately endergonic and kinetically feasible reactions with CS_2 in solution. Zr-based MXenes therefore are predicted to form a class of highly promising electrode materials for Li-ion batteries.

Acknowledgment

Research reported in this publication was supported by the King Abdullah University of Science and Technology (KAUST). AC is grateful for funding from the Lloyds Register Foundation, a charitable foundation helping to protect life and property by supporting engineering-related education, public engagement and the application of research.

References

[1] Novoselov, K. S.; Jiang, D.; Schedin, F.; Booth, T. J.; Khotkevich, V. V.; Morozov, S. V.; Geim, A. K. Two-Dimensional Atomic Crystals. *Proc. Natl. Acad. Sci. U.S.A.* **2005**, *102*, 10451–10453.

[2] Jeong, S.; Yoo, D.; Jang, J.-T.; Kim, M.; Cheon, J. Well-Defined Colloidal 2-D Layered Transition-Metal Chalcogenide Nanocrystals via Generalized Synthetic Protocols. *J. Am. Chem. Soc.* **2012**, *134*, 18233–18236.

[3] Cahangirov, S.; Topsakal, M.; Aktürk, E.; Şahin, H.; Ciraci, S. Two- and One-Dimensional Honeycomb Structures of Silicon and Germanium. *Phys. Rev. Lett.* **2009**, *102*, 236804.

[4] Novoselov, K. S.; Geim, A. K.; Morozov, S. V.; Jiang, D.; Zhang, Y.; Dubonos, S. V.; Grigorieva, I. V.; Firsov, A. A. Electric Field Effect in Atomically Thin Carbon Films. *Science* **2004**, *306*, 666–669.

[5] Castro Neto, A. H.; Guinea, F.; Peres, N. M. R.; Novoselov, K. S.; Geim, A. K. The Electronic Properties of Graphene. *Rev. Mod. Phys.* **2009**, *81*, 109–162.

[6] Novoselov, K. S.; Fal'ko, V. I.; Colombo, L.; Gellert, P. R.; Schwab, M. G.; Kim, K. A Roadmap for Graphene. *Nature* **2012**, *490*, 192–200.

[7] Tang, Q.; Zhou, Z. Graphene-Analogous Low-Dimensional Materials. *Prog. Mater. Sci.* **2013**, *58*, 1244–1315.

[8] Naguib, M.; Mochalin, V. N.; Barsoum, M. W.; Gogotsi, Y. 25th Anniversary Article: MXenes: A New Family of Two-Dimensional Materials. *Adv. Mater.* **2014**, *26*, 992–1005.

[9] Lei, J.-C.; Zhang, X.; Zhou, Z. Recent Advances in MXene: Preparation, Properties, and Applications. *Front. Phys.* **2015**, *10*, 276–286.

[10] Zhang, X.; Ma, Z.; Zhao, X.; Tang, Q.; Zhou, Z. Computational Studies on Structural and Electronic Properties of Functionalized MXene Monolayers and Nanotubes. *J. Mater. Chem. A* **2015**, *3*, 4960–4966.

[11] Naguib, M.; Gogotsi, Y. Synthesis of Two-Dimensional Materials by Selective Extraction. *Acc. Chem. Res.* **2015**, *48*, 128–135.

[12] Barsoum, M. W. *MAX Phases: Properties of Machinable Ternary Carbides and Nitrides*; Wiley-VCH, 2013.

[13] Zhang, X.; Xu, J.; Wang, H.; Zhang, J.; Yan, H.; Pan, B.; Zhou, J.; Xie, Y. Ultrathin Nanosheets of MAX Phases with Enhanced Thermal and Mechanical Properties in Polymeric Compositions: $Ti_3Si_{0.75}Al_{0.25}C_2$. *Angew. Chem. Int. Ed.* **2013**, *52*, 4361–4365.

[14] Hu, Q.; Sun, D.; Wu, Q.; Wang, H.; Wang, L.; Liu, B.; Zhou, A.; He, J. MXene: A New Family of Promising Hydrogen Storage Medium. *J. Phys. Chem. A* **2013**, *117*, 14253–14260.

[15] Lee, Y.; Hwang, Y.; Cho, S. B.; Chung, Y.-C. Achieving a Direct Band Gap in Oxygen Functionalized-Monolayer Scandium Carbide by Applying an Electric Field. *Phys. Chem. Chem. Phys.* **2014**, *16*, 26273–26278.

[16] Ma, Z.; Hu, Z.; Zhao, X.; Tang, Q.; Wu, D.; Zhou, Z.; Zhang, L. Tunable Band Structures of Heterostructured Bilayers with Transition-Metal Dichalcogenide and MXene Monolayer. *J. Phys. Chem. C* **2014**, *118*, 5593–5599.

[17] Gao, Y.; Wang, L.; Li, Z.; Zhou, A.; Hu, Q.; Cao, X. Preparation of MXene-Cu_2O Nanocomposite and Effect on Thermal Decomposition of Ammonium Perchlorate. *Solid State Sci.* **2014**, *35*, 62–65.

[18] Wang, F.; Yang, C.; Duan, C.; Xiao, D.; Tang, Y.; Zhu, J. An Organ-Like Titanium Carbide Material (MXene) with Multilayer Structure Encapsulating Hemoglobin for a Mediator-Free Biosensor. *J. Electrochem. Soc.* **2015**, *162*, B16–B21.

[19] Khazaei, M.; Arai, M.; Sasaki, T.; Estili, M.; Sakka, Y. The Effect of the Interlayer Element on the Exfoliation of Layered Mo_2AC (A = Al, Si, P, Ga, Ge, As or In) MAX Phases into Two-Dimensional Mo_2C Nanosheets. *Sci. Tech. Adv. Mater.* **2014**, *15*, 014208.

[20] Xie, Y.; Naguib, M.; Mochalin, V. N.; Barsoum, M. W.; Gogotsi, Y.; Yu, X.; Nam, K.-W.; Yang, X.-Q.; Kolesnikov, A. I.; Kent, P. R. C. Role of Surface Structure on Li-Ion Energy Storage Capacity of Two-Dimensional Transition-Metal Carbides. *J. Am. Chem. Soc.* **2014**, *136*, 6385–6394.

[21] Er, D.; Li, J.; Naguib, M.; Gogotsi, Y.; Shenoy, V. B. Ti_3C_2 MXene as a High Capacity Electrode Material for Metal (Li, Na, K, Ca) Ion Batteries. *ACS Appl. Mater. Interfaces* **2014**, *6*, 11173–11179.

[22] Tang, Q.; Zhou, Z.; Shen, P. Are MXenes Promising Anode Materials for Li Ion Batteries? Computational Studies on Electronic Properties and Li Storage Capability of Ti_3C_2 and $Ti_3C_2X_2$ (X = F, OH) Monolayer. *J. Am. Chem. Soc.* **2012**, *134*, 16909–16916.

[23] Lee, Y.; Cho, S. B.; Chung, Y.-C. Tunable Indirect to Direct Band Gap Transition of Monolayer Sc_2CO_2 by the Strain Effect. *ACS Appl. Mater. Interfaces* **2014**, *6*, 14724–14728.

[24] Zhao, S.; Kang, W.; Xue, J. Role of Strain and Concentration on the Li Adsorption and Diffusion Properties on Ti_2C Layer. *J. Phys. Chem. C* **2014**, *118*, 14983–14990.

[25] Sun, D.; Wang, M.; Li, Z.; Fan, G.; Fan, L.-Z.; Zhou, A. Two-Dimensional Ti_3C_2 as Anode Material for Li-Ion Batteries. *Electrochem. Commun.* **2014**, *47*, 80–83.

[26] Xie, Y.; Kent, P. R. C. Hybrid Density Functional Study of Structural and Electronic Properties of Functionalized $Ti_{n+1}X_n$ (X = C, N) Monolayers. *Phys. Rev. B* **2013**, *87*, 235441.

[27] Eames, C.; Islam, M. S. Ion Intercalation into Two-Dimensional Transition-Metal Carbides: Global Screening for New High-Capacity Battery Materials. *J. Am. Chem. Soc.* **2014**, *136*, 16270–16276.

[28] Zhao, S.; Kang, W.; Xue, J. Manipulation of Electronic and Magnetic Properties of M_2C (M = Hf, Nb, Sc, Ta, Ti, V, Zr) Monolayer by Applying Mechanical Strains. *Appl. Phys. Lett.* **2014**, *104*, 133106.

[29] Enyashin, A.; Ivanovskii, A. Two-Dimensional Titanium Carbonitrides and Their Hydroxylated Derivatives: Structural, Electronic Properties and Stability of MXenes $Ti_3C_{2-x}N_x(OH)_2$ from DFTB Calculations. *J. Solid State Chem.* **2013**, *207*, 42–48.

[30] Hu, J.; Xu, B.; Ouyang, C.; Yang, S. A.; Yao, Y. Investigations on V_2C and V_2CX_2 (X = F, OH) Monolayer as a Promising Anode Material for Li Ion Batteries from First-Principles Calculations. *J. Phys. Chem. C* **2014**, *118*, 24274–24281.

[31] Yang, J.; Naguib, M.; Ghidiu, M.; Pan, L.-M.; Gu, J.; Nanda, J.; Halim, J.; Gogotsi, Y.; Barsoum, M. W. Two-Dimensional Nb-Based M_4C_3 Solid Solutions (MXenes). *J. Am. Ceram Soc.* **2015**, DOI:10.1111/jace.13922.

[32] Naguib, M.; Bentzel, G. W.; Shah, J.; Halim, J.; Caspi, E. N.; Lu, J.; Hultman, L.; Barsoum, M. W. New Solid Solution MAX Phases: $(Ti_{0.5}, V_{0.5})_3AlC_2$, $(Nb_{0.5}, V_{0.5})_2AlC$, $(Nb_{0.5}, V_{0.5})_4AlC_3$ and $(Nb_{0.8}, Zr_{0.2})_2AlC$. *Mater. Res. Lett.* **2014**, *2*, 233–240.

[33] Khazaei, M.; Arai, M.; Sasaki, T.; Estili, M.; Sakka, Y. Trends in Electronic Structures and Structural Properties of MAX Phases: A First-Principles Study on M_2AlC (M = Sc, Ti, Cr, Zr, Nb, Mo, Hf, or Ta), M_2AlN, and Hypothetical M_2AlB Phases. *J. Phys.: Condens. Matter* **2014**, *26*, 505503.

[34] Li, Z.; Wang, L.; Sun, D.; Zhang, Y.; Liu, B.; Hu, Q.; Zhou, A. Synthesis and Thermal Stability of Two-Dimensional Carbide MXene Ti_3C_2. *Mater. Sci. Eng. B* **2015**, *191*, 33–40.

[35] Xie, Y.; DallAgnese, Y.; Naguib, M.; Gogotsi, Y.; Barsoum, M. W.; Zhuang, H. L.; Kent, P. R. C. Prediction and Characterization of MXene Nanosheet Anodes for Non-Lithium-Ion Batteries. *ACS Nano* **2014**, *8*, 9606–9615.

[36] Kresse, G.; Joubert, D. From Ultrasoft Pseudopotentials to the Projector Augmented-wave Method. *Phys. Rev. B* **1999**, *59*, 1758–1775.

[37] Perdew, J. P.; Burke, K.; Ernzerhof, M. Generalized Gradient Approximation Made Simple. *Phys. Rev. Lett.* **1996**, *77*, 3865–3868.

[38] Mills, G.; Jónsson, H.; Schenter, G. K. Reversible Work Transition State Theory: Application to Dissociative Adsorption of Hydrogen. *Surf. Sci.* **1995**, *324*, 305–337.

[39] All experimental values taken form the Nation Institute of Standards and Technology database: webbook.nist.gov.

[40] Bouhemadou, A.; Khenata, R.; Chegaar, M. Structural and Elastic Properties of Zr_2AlX and Ti_2AlX (X = C and N) under Pressure Effect. *Eur. Phys. J. B* **2007**, *56*, 209–215.

[41] Naguib, M.; Halim, J.; Lu, J.; Cook, K. M.; Hultman, L.; Gogotsi, Y.; Barsoum, M. W. New Two-Dimensional Niobium and Vanadium Carbides as Promising Materials for Li-Ion Batteries. *J. Am. Chem. Soc.* **2013**, *135*, 15966–15969.

[42] West, W. A.; Menzies, A. W. C. The Vapor Pressures of Sulphur between 100° and 550° with Related Thermal Data. *J. Phys. Chem.* **1928**, *33*, 1880–1892.

[43] Rhodes, C.; Riddel, S. A.; West, J.; Williams, B.; Hutchings, G. J. The Low-Temperature Hydrolysis of Carbonyl Sulfide and Carbon Disulfide: A Review. *Catal. Today* **2000**, *59*, 443–464.

[44] Smeulders, M. J.; Barends, T. R. M.; Pol, A.; Scherer, A.; Zandvoort, M. H.; Udvarhelyi, A.; Khadem, A. F.; Menzel, A.; Hermans, J.; Shoeman, R. L.; Wessels, H. J. C. T.; van den Heuvel, L. P.; Russ, L.; Schlichting, I.; Jetten, M. S. M.; Op den Camp, H. J. M. Evolution of a New Enzyme for Carbon Disulphide Conversion by an Acidothermophilic Archaeon. *Nature* **2011**, *478*, 412–416.

[45] Kaminskii, B.; Prokof'eva, G.; Plygunov, A.; Galitskii, P. Manufacture of Zirconium and Hafnium Sulfide Powders. *Sov. Powder Metall. Met. Ceram.* **1973**, *12*, 521–524.

[46] Donahue, J. P. Thermodynamic Scales for Sulfur Atom Transfer and Oxo-for-Sulfido Exchange Reactions. *Chem. Rev.* **2006**, *106*, 4747–4783.

[47] Oledzka, M.; Ramanujachary, K. V.; ; Greenblatt, M. New Low-Dimensional Quaternary Sulfides $NaCuMS_2$ (M = Mn, Fe, Co, and Zn) with the $CaAl_2Si_2$-Type Structure: Synthesis and Properties. *Chem. Mater.* **1998**, *10*, 322–328.

[48] Güler, H.; Kurtuluş, F. The Synthesis of NiS, ZnS and SrS Through Solid-Gas Reaction of Sulfidizing Gas Mixture. *J. Sulfur Chem.* **2006**, *27*, 37–48.

[49] Mouallem-Bahout, M.; Peña, O.; Carel, C.; Ouammou, A. Electrical and Magnetic Properties of New Mixed Transition Metal Sulfides $BaKCu_3MS_4$ (M=Mn, Co, Ni). *J. Solid State Chem.* **2001**, *157*, 144–148.

Table of Contents Graphic